QUANTITATIVE INVESTIGATION OF QUANTUM CONFINED $CsPbBr_3$ NANOCRYSTALS TO FURTHER UNDERSTAND SIZE-DEPENDENT PROPERTIES

A Thesis

by

JOSEPH K. PUTHENPURAYIL

Submitted to the Graduate and Professional School of
Texas A&M University
in partial fulfillment of the requirements for the degree of

MASTER OF SCIENCE

Chair of Committee,	Dong Hee Son
Committee Members,	Simon North
	Matthew Sheldon
	Alexei Sokolov
Head of Department,	Simon North

December 2022

Major Subject: Chemistry

ABSTRACT

The absorption cross section of lead halide perovskite nanocrystals is important for understanding their photophysical properties, especially those depending on the density of photoexcited charge carriers. Despite its importance, there are large discrepancies among the reported absorption cross section values determined employing different methods. Here, we measured the absorption cross section of $CsPbBr_3$ quantum dots of varying sizes using elemental analysis and transient absorption (TA) saturation methods and compared with the previously reported values determined from elemental analysis and transient photoluminescence (PL) saturation methods. Careful comparison indicates that the reliable absorption cross section of lead halide perovskite QDs are obtained from both elemental analysis and TA saturation methods, while many previously reported values determined from the PL saturation method underestimate the absorption cross section. This work further quantifies properties of the $CsPbBr_3$ material to allow for further ease in predicting the material's behavior when quantum confined and shows further application of transient absorption methodologies to understand the excitonic properties and processes exhibited.

ACKNOWLEDGEMENTS

Thanks to my friends, family, and labmates.

CONTRIBUTORS AND FUNDING SOURCES

Contributors

This work was supervised by a thesis committee consisting of Professor Dong Hee Son, Professor Matthew Sheldon, and Professor Simon North of the Department of Chemistry, and Professor Alexei Sokolov of the Department of Physics.

The lead halide perovskite samples in Chapter 2 were synthesized by Dr. Tian Qiao, Xueting Tang, and myself of the Department of Chemistry. TEM images from Chapter 2 were obtained by Dr. Tian Qiao and Xueting Tang of the Department of Chemistry. Some ultrafast measurements from Chapter 2 were performed in collaboration between myself and Dr. Oscar Cheng of the Department of Chemistry. All other work for this thesis was completed by the student independently.

Funding Sources

Graduate study was supported by a fellowship from Texas A&M University.

NOMENCLATURE

$CsPbBr_3$	Cesium Lead Bromide
ϵ_λ	Extinction Coefficient at a given Wavelength
σ_λ	Absorption Cross Section at a given Wavelength
N_A	Avogadro's Number
A	Absorbance
QD	Quantum Dot
C_{QD}	Particle Concentration
b, l	Pathlength
ICP-MS	Inductively Coupled Plasma Mass Spectrometry
PL	Photoluminescence
TA	Transient Absorption
TEM	Transmission Electron Microscopy
n	Average Number of Photoexcited Excitons
CCD	Charge Coupled Device
BBO	β-Barium Borate
FWHM	Full Width at Half Maximum
V	Volume
L	Edge Length
N_{Pb}	Number of Lead Ions
t_l	Long Time after Excitation
I_{PL}	Photoluminescence Intensity

<N>	Average Number of Photons Absorbed per Quantum Dot
F_{ph}	Photon Fluence
$\Delta OD(t)$	Transient Absorption Signal; Change in Optical Density Effected by the Pump Pulse at a given time after Pump Excitation
$\lvert \Delta OD(t) \rvert_{norm}$	Absolute Value and Normalized Transient Absorption Signal
ns	nanoseconds
ps	picoseconds
nm	nanometer
μm	micrometer
F_0	Incident Pump Photon Fluence on Front of Sample Cell

TABLE OF CONTENTS

Page

LIST OF FIGURES

Page

LIST OF TABLES

Page

1. INTRODUCTION

Cesium lead bromide ($CsPbBr_3$) perovskite nanocrystals are a kind of semiconductor quantum dots, and this material has been of significant interest due to its optoelectronic properties. $CsPbBr_3$ and other cesium lead halide materials show a wide range of emission and absorption tuning with size, morphology, and composition[1, 2], high photoluminescence (PL) quantum yields[1, 3, 4], and large carrier diffusion lengths[3]. These properties lend it to applications such as LEDs[5], lasers[6, 7], and solar cells[8-10] as well as further photovoltaic devices.

Better understanding this material as well as exploring its properties when taken to the nanoscale helps further drive its use cases and our knowledge of fundamental semiconductor behaviors. Recently, synthesis of homogenous, quantum-confined $CsPbBr_3$ cubic nanocrystals has been achieved allowing for further investigation of their excitonic properties.[4] A material is considered quantum confined when its physical size is smaller than its exciton Bohr diameter. The exciton Bohr radius gives the separation between the electron and hole in an exciton. In $CsPbBr_3$, the exciton Bohr diameter is ~ 7 nm, so cubic $CsPbBr_3$ particles with edge lengths smaller than 7 nm can be considered quantum confined.[11] When a particle is subject to quantum confinement it shows many size dependent properties differing from its behavior as a bulk material.[4]

One property of interest, especially for light-matter interactions, is the absorption cross section. The absorption cross section of a material gives the probability of an absorption process, allowing for prediction of how many excitations a certain amount of

light could produce when shone on an area of a colloidal solution or film. It is directly related to the extinction coefficient by the following relation, with extinction coefficient (ϵ_λ) in M^{-1} cm^{-1} and absorption cross section (σ_λ) in cm^2 and with N_A being Avogadro's number.[12] Beer's law further relates the extinction coefficient to absorbance (A_λ) of a particle concentration (C_{QD}) accounting for path length (b).

$$\sigma_\lambda = \frac{2303\ \epsilon_\lambda}{N_A}\ , A_\lambda = \epsilon_\lambda b C_{QD}$$

The extinction coefficient is also useful on its own for establishing the concentration of a material using Beer's law. The absorption cross section can be found by working from Beer's law to the absorption cross section using solutions of known concentration, but in the case of hot injection synthesized QDs, this method becomes difficult as yields are not consistent and the dots undergo several washing processes, making it hard to prepare known concentration stocks. Establishing an absorption cross section becomes useful for then calculating the concentration from the absorbance of the synthesized solution or a dilution of the final products.[12]

Another approach to understanding the absorption cross section of a colloidal solution of particles of simple, symmetric geometry relies on the use of inductively coupled plasma mass spectrometry (ICP-MS) to perform elemental analysis on the particles to establish concentrations of atoms in solution, relate back to concentration of particles in solution, knowing particle size and shape, and extract the extinction

coefficient from UV-Vis spectroscopic measurements of the particles' absorption before their careful, quantitative digestion and dilution during the preparation for ICP-MS.[13]

A third approach to understanding the absorption cross section of a colloidal solution of QDs is via analysis of PL or transient absorption (TA) data based on Poisson distributions, more directly measuring the probability of absorption producing a signal.[14, 15] This approach monitors the saturation of the transient absorption signal intensity at the peak of exciton absorption or transient photoluminescence intensity with increasing excitation fluence. This kind of approach does not require detailed knowledge of particle geometry, unlike the ICP-MS approach, which can be beneficial for more anisotropic or unusual particle morphologies. Additionally, single particle methods can be used to measure absorption cross sections.[16]

Further interest in the perovskite material drives other investigations into its properties. A collaborative measurement was performed to confirm bright and dark exciton splitting in various morphologies of $CsPbBr_3$.[17] Additional measurements were carried out in a hot electron photocatalytic reduction scheme.[18] Transient absorption measurements were also performed to investigate the role of formate in a larger charge transfer scheme.[19]

2. ON THE DETERMINATION OF ABSORPTION CROSS SECTION OF COLLOIDAL LEAD HALIDE PEROVSKITE QUANTUM DOTS*

2.1. Introduction

The lead halide perovskite materials have been of great interest in recent years for photovoltaic[9, 10, 20, 21] and optoelectronic[6, 22-25] applications due to their optical, electronic and transport properties surpassing those of many other semiconductor materials. Colloidal nanocrystals of these materials are also extensively studied as the superior alternative to many other semiconductor nanocrystals used for decades as the source of photons for their facile chemical tuning of bandgap and high luminescence quantum yield approaching unity in some cases.[1, 26] Furthermore, the controllable dimensionality (0D-2D) and the quantum confinement achievable in many lead halide perovskites render them highly attractive as a new family of quantum confined semiconductor nanocrystals applicable as the light harvester or emitter of photons.[2, 6, 27] Low nonradiative loss of the photoexcited exciton and relatively large exciton Stokes shift in lead halide perovskite nanocrystals were considered beneficial for photonic applications such as lasing (or optical gain) with low threshold.[6]

For such applications, information on the average number of photoexcited excitons (n) in the nanocrystal at the given excitation intensity is important, especially for $n>1$.[6, 13, 28,

* Reproduced from Puthenpurayil, J.; Cheng, O. H. C.; Qiao, T.; Rossi, D.; Son, D. H., On the determination of absorption cross section of colloidal lead halide perovskite quantum dots. *J. Chem. Phys.* **2019,** *151* (15)., with the permission of AIP Publishing

[29] For instance, the radiative exciton recombination competes with *n*-dependent nonradiative decay channel such as Auger relaxation, requiring the knowledge of *n* in order to understand such dynamics. Often, one estimates *n* from the absorption cross section (σ) and the excitation fluence assuming that σ is not very sensitive to the excitation density, which is a reasonable assumption at significantly above the bandgap with sufficiently large density of state. In principle, one can obtain the average absorption cross section of the nanocrystals from the elemental analysis in conjunction with the information of the size (volume), shape and stoichiometric composition of the nanocrystal if the size and shape of the nanocrystals are sufficiently uniform and well-defined. Such strategy has been successfully used for measuring the absorption cross section of various binary quantum dots (QDs).[12, 30-33] Another approach determining the average absorption cross section is analyzing the saturation of the transient absorption (TA) intensity at the peak of exciton absorption or transient photoluminescence (PL) intensity with increasing excitation fluence.[14, 34, 35] Compared to the method based on elemental analysis, determination of the absorption cross section from the saturation of TA or PL intensity does not require information on the volume of the nanocrystals. This is an important advantage over the elemental analysis method, especially for the structures with anisotropic morphology where the determination of the volume is not always straightforward. It is worth mentioning that the absorption cross section of isolated single nanocrystals has also been measured via photothermal imaging of individual particles.[16] Earlier studies in binary QDs have shown that both the elemental analysis and saturation approaches result in comparable absorption cross section values.[32, 34]

In the case of lead halide perovskite QDs, the absorption cross sections reported so far are spread in a wide range differing by an order of magnitude depending on the method employed. Hens and coworkers employed the elemental analysis method to determine the size-dependent absorption cross section of $CsPbBr_3$ QDs in the size range of 4 - 11 nm, which are similar to those of CdSe QDs of the same volume.[12, 13] On the other hand, several other studies that employed the transient PL intensity saturation method reported scattered values that are also an order of magnitude smaller than those of Hens and coworkers for QDs of similar volume.[14, 35] It is not yet clear why there is such a large discrepancy between the two measurements. However, an order of magnitude smaller value from the PL intensity saturation method is quite unusual, since the QDs of many different materials exhibit absorption cross sections of the same order of magnitude for a given volume at the energies significantly above the bandgap.[12, 30, 36]

In this work, we measured the absorption cross section of $CsPbBr_3$ QDs of varying sizes employing both elemental analysis and transient absorption (TA) saturation methods and compared with the previously reported data. From this comparative analysis, we obtained reliable absorption cross section values of $CsPbBr_3$ QDs as a function of size in the strongly confined regime. Both the elemental analysis and TA saturation methods gave similar results that are also very close to the result of Hens and coworkers, suggesting the higher reliability of the absorption cross section determined from these two methods than the transient PL saturation method. The results from this study also show that the TA saturation method can reliably determine the absorption cross section of perovskite

nanocrystals without knowledge of the volume, which will be particularly useful for nanocrystals with complex morphologies.

2.2. Experimental Section

2.2.1. Sample Synthesis and Characterization

Elemental composition of Cs and Pb was determined using inductively coupled plasma mass spectrometry (ICP-MS). The samples for the elemental analysis were prepared by first measuring the absorption spectra of the QD solution dispersed in hexane, which was subsequently dried and digested in 70% aqueous solution of nitric acid. Appropriate dilutions were made using 1% nitric acid. ICP-MS measurements were made with a NexION 300 ICP-MS instrument. The calibration curves used for the determination of the ion concentration of the samples were obtained using the standard solutions (Sigma Aldrich, 1000 mg/L stock) which were diluted to a known dilution factor. Indium and bismuth were used as internal standards for Cs and Pb, respectively.

2.2.2. Elemental Analysis

Elemental composition of Cs and Pb was determined using inductively coupled plasma mass spectrometry (ICP-MS). The samples for the elemental analysis were prepared by first measuring the absorption spectra of the QD solution dispersed in hexane, which was subsequently dried and digested in 70% aqueous solution of nitric acid. Appropriate dilutions were made using 1% nitric acid. ICP-MS measurements were

made with a NexION 300 ICP-MS instrument. The calibration curves used for the determination of the ion concentration of the samples were obtained using the standard solutions (Sigma Aldrich, 1000 mg/L stock) which were diluted to a known dilution factor. Indium and bismuth were used as internal standards for Cs and Pb, respectively.

2.2.3. Transient Absorption Measurement

Transient absorption measurements were performed on a home-built pump-probe transient absorption spectrometer. The 400 nm pump was generated by doubling the 800 nm output (80fs, 3kHz) of a Titanium-sapphire amplifier (KM Laboratories) with a 300 μm-thick β-barium borate (BBO) crystal whose fluence was controlled by a pair of linear polarizer and a half waveplate.[37] The white light supercontinuum probe was generated by focusing a few μJ of 800 nm beam on a 1 mm-thick CaF2 window.[37] Transient absorption data at a chosen probe wavelength were recorded using a pair of amplified Si photodiodes and a monochromator (Newport, Oriel Cornerstone 130), in conjunction with Boxcar gated integrators. QD samples dispersed in ~30 ml of cyclohexane were circulated through a quartz flow cell with 2 mm pathlength to avoid any potential photodegradation. Cyclohexane was used for the TA measurement due to its slower evaporation rate compared to hexane allowing for easier control of the constant sample concentration during the prolonged measurement using the liquid flow cell. The full width at half maximum (FWHM) beam diameter of 400 nm pump beam was ~230 μm, which was determined by using the razor blade method.[38] The FWHM of the weaker probe beam (~20 μm) was measured by directly imaging the probe beam on a

CCD camera (DMK21BU04, The Imaging Source) at the sample position. The power of the 400 nm pump beam was measured with an Ophir Nova power meter and Ophir 3A-P-SH-VI sensor. For the accurate measurement of the power of 400 nm pump beam with minimal contamination from 800 nm beam, two sets of dielectric mirrors selectively reflecting 400 nm and transmitting 800 nm were used after the BBO crystal. Any residual 800 nm light reaching to the power meter was corrected for by separately measuring the power of leaking 800 nm beam in the absence of BBO crystal in the beam path. Further details on the pump fluence determination are in Supplementary Material.

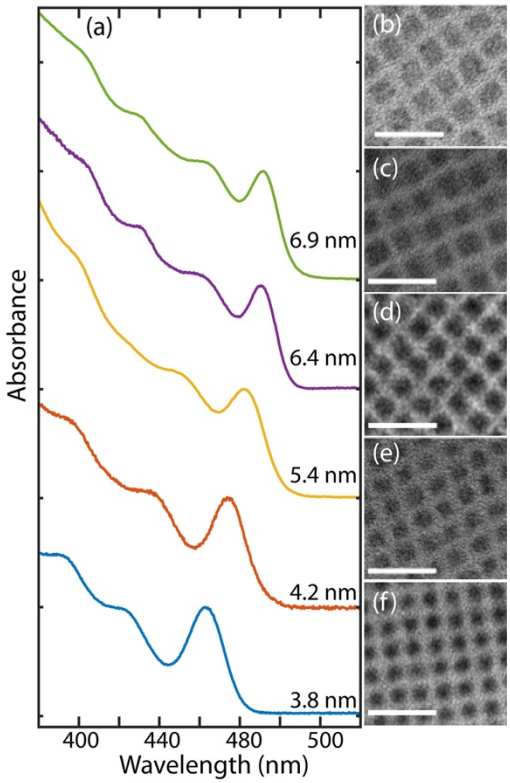

Figure 2.1. (a) Size-dependent absorption spectra and (b-f) TEM images of the $CsPbBr_3$ quantum dots (QDs) used in this study. The size shown is the edge length of the QDs. Scale bar is 20 nm.

2.3. Results and Discussion

The absorption cross section of the strongly confined $CsPbBr_3$ QDs dispersed in hexane was determined employing two different methods in this work, i.e. elemental analysis and saturation of transient absorption (TA). The method based on the elemental analysis is effective when the volume and the elemental composition of the QDs are readily determined. Since the $CsPbBr_3$ QDs synthesized in this study exhibit highly uniform size and morphology, the determination of the volume of the QD from the analysis of TEM images is relatively straightforward. The absorption cross section of the QDs was determined using the Beer's law from the measured absorption spectrum (A_λ) and molar concentration of QDs (c_{QD}) in the sample solution determined from the elemental analysis and the volume of the QD. The absorption cross section (σ_λ) was calculated from the molar absorption coefficient (ϵ_λ) with the conversion factor of $2303/N_A$, where N_A is Avogadro's number.[12]

$$A_\lambda = \epsilon_\lambda b c_{QD},\ \sigma_\lambda = \epsilon_\lambda \frac{2303}{N_A} \quad (1)$$

In this approach, the number of Pb ions (N_{Pb}) contained in the QD of volume ($V=L^3$) was first determined by considering the cube-shaped QDs with the surface terminated with Br^- and passivated with oleylammonium ion using the edge length (L) obtained from the TEM images (Supplementary Material, Table S1) c_{QD} was calculated from N_{Pb} and the molar concentration of Pb ions in the QD sample solution (c_{Pb}) determined from the elemental analysis. Since the stoichiometric ratio Cs:Pb:Br in $CsPbBr_3$ QDs deviates from

1:1:3 depending on the size and surface terminating element of the QD especially for Cs and Br, we chose Pb to determine the concentration of QDs that is considered less sensitive to the detailed surface structure.[13, 39, 40]

In Fig. 2, the absorption cross sections of $CsPbBr_3$ QDs at 400 nm (σ_{400}) determined using the method described above are plotted. For comparison, the result from the earlier work by Hens and coworkers,[13] who employed the elemental analysis approach using slightly different data analysis method, are also shown alongside σ_{400} determined by TA saturation method as will be discussed later. σ_{400} of the QDs measured employing the elemental analysis approach from the two different studies (this work and Ref. [13]) are similar to each other for the QDs of comparable sizes, indicating the consistency of this method in determining the absorption cross section of $CsPbBr_3$ QDs. The small difference in the values of σ_{400} may partially reflect the difference in the uncertainty and distribution of the QD size in the samples used in these two studies. The absorption cross section determined from the elemental analysis depends directly on the number of atoms within the QD counted for each element, which varies with the size and shape of the nanocrystal and surface termination. Therefore, despite the general applicability of the elemental analysis-based method for the measurement of absorption cross section, its accuracy depends strongly on the quality of information on the size and shape of the nanocrystal and its surface structure.

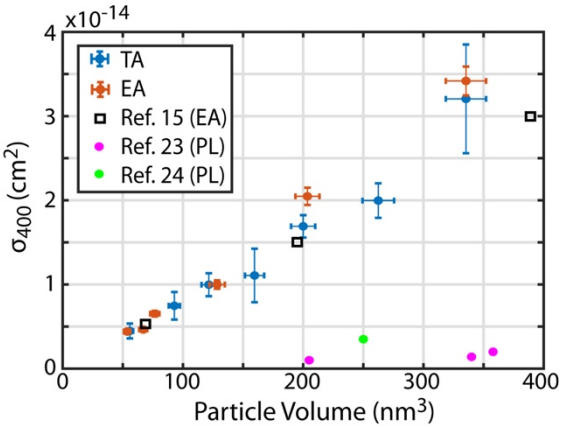

Figure 2.2. The absorption cross section of $CsPbBr_3$ QDs of different sizes at 400 nm (σ_{400}) determined from elemental analysis (EA) and transient absorption (TA) in this work. The error bar on the x-axis represents maximum of 5% estimated dispersity in the edge length of the QDs. For comparison, the values reported in Ref. [13] from EA are also shown with the values in Ref. [14] and Ref. [35] from transient photoluminescence (PL) measurements.

The alternative methods determining the absorption cross section of the QDs that do not require such information rely on the saturation behavior of transient photoluminescence (PL) intensity or transient absorption (TA) bleach signal. In the case of transient PL intensity saturation, it should exhibit the saturation behavior described by the following equation, if the number of photons absorbed by the QD can be described by Poisson statistics.

$$I_{PL}(t_l) = a(1 - e^{-\langle N \rangle}) = a(1 - e^{-F_{ph} * \sigma_\lambda}) \quad (2)$$

$I_{PL}(t_l)$ is the transient PL intensity at a sufficiently long time t_l after the excitation, at which the PL decay dynamics reflect the decay of only single excitons. $\langle N \rangle$ is the average number of photons absorbed per QD at the given excitation fluence. F_{ph} and σ_λ are the

photon fluence (in photons/cm^2) and absorption cross section (in cm^2) at the excitation wavelength respectively. a is a normalization constant.[6, 14] For the lead halide perovskite nanocrystals, the majority of the reported absorption cross sections were determined by analyzing the PL intensity saturation including $CsPbBr_3$, $CsPbI_3$, and $CsPbBr_xI_{3-x}$.[6, 14, 35] Fig. 2 includes the previously reported σ_{400} of $CsPbBr_3$ QDs determined using the PL saturation method for comparison. The numerical values of σ_{400} from this study and the earlier studies are tabulated in Supplementary Material (Table S2). Notably, the absorption cross section of $CsPbBr_3$ QDs determined from the PL intensity saturation method are much smaller and scattered significantly between different measurements. In principle, both the elemental analysis and PL intensity saturation method should give comparable absorption cross sections. While the origin of such a large discrepancy existing in the literature is not clear, we note that PL saturation method can easily underestimate the absorption cross section when a spatially nonuniform excitation beam is used as will be discussed later.

Another way to determine the absorption cross section without the QD size information is to analyze the bleach signal at the peak of exciton absorption in the transient absorption (TA) data, which is methodologically similar to the PL intensity saturation method. Both have the same underlying assumption of the applicability of the Poisson distribution for the number of photons absorbed in the QDs, therefore sharing the similar equation relating the absorption cross section to the signal saturation curve.[14] However, TA signal saturation has been much less frequently used than the PL saturation method for the perovskite QDs. In this study, taking advantage of recent progress in synthesis of

highly uniform and stable QDs under prolonged TA measurement condition[37, 41], we determined σ_{400} of $CsPbBr_3$ QDs using the TA saturation method and compared with those determined by elemental analysis. For this purpose, TA signal probed at the peak of the exciton absorption, $\Delta OD(t)$, was measured with 400 nm pump for each QD as a function of excitation fluence.

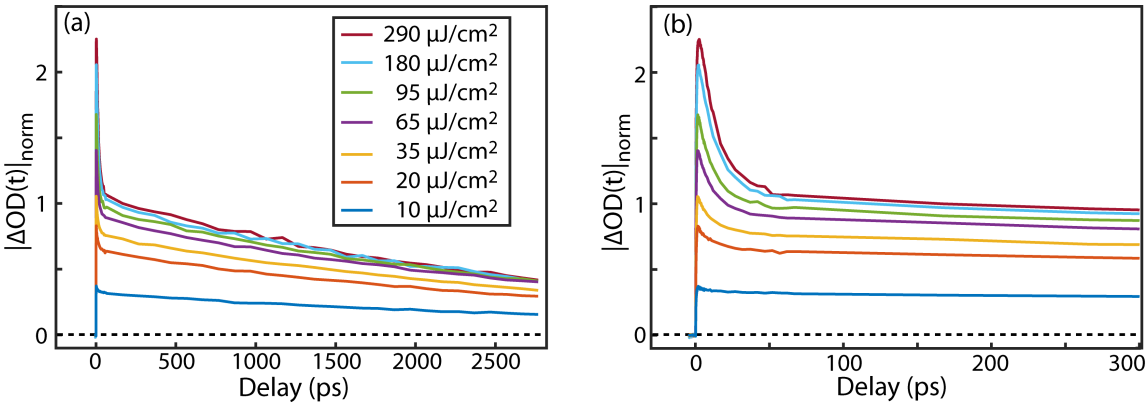

Figure 2.3. (a) $|\Delta OD(t)|_{norm}$ of $CsPbBr_3$ QDs (L=6.9 nm) probed at the peak of exciton absorption normalized to $|\Delta OD(200\ ps)|$ at the saturating pump fluence. (b) Early-time dynamics showing the rapid decay from Auger recombination at the higher pump fluences more clearly.

Fig. 3(a) shows the normalized $|\Delta OD(t)|$, $|\Delta OD(t)|_{norm}$, for the $CsPbBr_3$ QDs with the edge length of L=6.9 nm at varying pump fluences. The data in Fig. 3(a) are normalized to $|\Delta OD(200\ ps)|$ at the saturating pump fluence. The pump fluence shown is the average pump fluence under the probe beam area, defined as the circular area with the diameter of full width at half maximum (fwhm) of the probe beam (~20 μm). In this study, fwhm of the pump beam (~230 μm) was much larger than that of the probe beam ensuring relatively homogeneous excitation fluence under the probed area. The data for the QDs of other sizes are in Supplementary Material. The early-time dynamics of $|\Delta OD(t)|$ shown more clearly

in Fig. 3(b) exhibit a rapidly decaying component on the time scale of several tens of ps, which becomes more prominent as the pump fluence increases due to the Auger decay of multiple excitons. After the completion of the Auger decay, the slow decay occurs on the time scale of ~5 ns reflecting the decaying of the remaining single exciton, which is nearly independent of the pump fluence.

Fig. 4 shows $|\Delta OD(200\ ps)|_{norm}$ for the QDs of four different sizes as a function of pump fluence extracted from $|\Delta OD(t)|_{norm}$ such as shown in Fig. 3 for the analysis of their saturation behavior. The curves are then fit to a model as will be discussed shortly. Additional data for other sizes and fit to a model are in Supplementary Materials. We chose 200 ps as the sufficiently long pump-probe delay time (t_l) that ensures the completion of Auger decay so that every photoexcited QD contributes equally to the TA signal regardless of the number of the initially excited excitons. Since the dynamics of the slow decay component in the TA data is nearly independent of the fluence, the TA signal saturation curve is insensitive to the chosen t_l as long as t_l is sufficiently long.

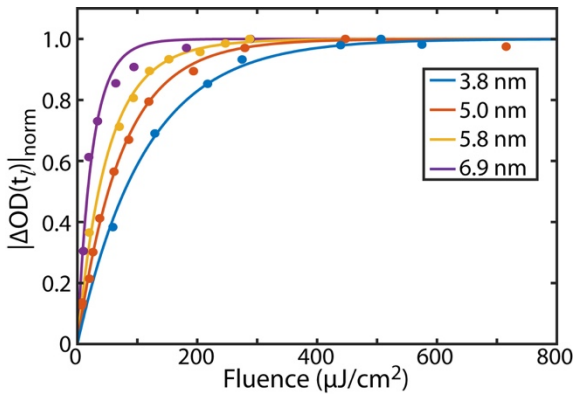

Figure 2.4 $|\Delta OD(t_l)|_{norm}$ as a function of pump fluence for $CsPbBr_3$ QDs of different sizes at t_l=200 ps. The curves are the best fit to Eq. (4).

For the optically dilute samples, $|\Delta OD(t_l)|_{norm}$ should exhibit the pump photon fluence dependence of Eq. (3) similar to the case of PL intensity, where F_{ph} is the photon fluence of the pump beam under the probe beam area.

$$|\Delta OD(t_l)|_{norm} = 1 - e^{-\langle N \rangle} = 1 - e^{-F_{ph} * \sigma_\lambda} \quad (3)$$

On the other hand, for the samples with significant absorbance at the pump wavelength, the attenuation of the pump beam through the sample that lowers the average photon fluence should be considered in the analysis of the saturation of $|\Delta OD(t_l)|_{norm}$. For the sample solution in a cell of pathlength l exhibiting the absorbance of A_l at the pump wavelength, the photon fluence at location x along the pathlength decays exponentially as $F_{ph}(A_l, x, l, F_0) = F_0 \cdot 10^{-A_l(x/l)}$, where F_0 is the incident pump photon fluence impinging on the sample. This modifies the dependence of $|\Delta OD(t_l)|_{norm}$ on F_0 as shown in Eq. (4).

$$|\Delta OD(t_l)|_{norm} = \frac{-E_1(\sigma_\lambda \cdot F_0 \cdot 10^{-A_l}) + E_1(\sigma_\lambda \cdot F_0)}{A_l \cdot ln(10)} + 1 \,, \quad E_1(x) = \int_x^\infty \frac{e^{-u}}{u} du \quad (4)$$

While this correction is not necessary for the PL measurement that can be made easily with optically dilute samples, it is needed for TA measurements that often uses samples of higher absorption. In this study, where the absorbance of the sample at 400 nm was 0.2 - 0.5, using Eq. (3) underestimates the absorption cross section up to factor of ~2. The curves in Fig. 4 are fits of the experimental data to Eq. (4). The quality of the fit in Fig. 4 is generally very good. While the fit is slightly worse in 6.9 nm QD than others, it may be

due to variation of the quality of sample rather than the failure of the Poisson statistics of photon absorption in this size. The derivation of Eq. (4) is in Supplementary Material. σ_{400} of $CsPbBr_3$ QDs of different sizes determined from the fit in Fig. 4 are also shown in Fig. 2 for comparison. σ_{400} determined using the TA saturation method is in good agreement with the result from the elemental analysis of this study and the earlier work by Hens and coworkers.[13] The consistency of the values of σ_{400} from this comparison indicates that the reliable absorption cross section of $CsPbBr_3$ QDs can be obtained from both the elemental analysis and TA saturation method. The wavelength-dependent absorption cross section (σ_λ) of $CsPbBr_3$ QDs of several different sizes in the spectral range of 350-550 nm based on σ_{400} values determined from the analysis of TA saturation are plotted in Fig. S1 of the Supplementary Material.

It is puzzling that the reported absorption cross section of various lead halide perovskite nanocrystals determined using the transient PL saturation method are much smaller than those from the elemental analysis and TA saturation method. For instance, Ref. [14] reported σ_{400} of 1.0×10^{-15} cm^2 for $CsPbBr_3$ QDs with L=5.9 nm (V=205 nm^3), which is more than an order of magnitude smaller than from this study as compared in Fig. 2. In the case of $CsPbI_3$, QDs, σ_{400} in the range of $1\text{-}1.3 \times 10^{-14}$ cm^2 was reported for QDs of L=11.2-11.4 nm,[14, 35, 42] which is also more than an order of magnitude smaller than what we determined from the elemental analysis for the QDs of comparable size in a separate measurement (σ_{400} = ~2.6×10^{-13} cm^2). While the reason for such discrepancy is uncertain, we note that the use of typical laser light with Gaussian beam profile on the sample cell larger than the beam size can underestimate the absorption cross section when

the entire PL signal is measured without spatial resolution. Because of the spatially varying PL saturation from the spatially inhomogeneous excitation intensity on the sample, the PL signal can appear to saturate more slowly when the entire PL signal is detected. For this reason, spatially resolved PL intensity measurement is required for an accurate analysis of the PL intensity vs excitation density when the excitation beam size is smaller than the size of the sample cell.[43]

Now we discuss the factors that can potentially affect the measurement of the absorption cross section via elemental analysis method more significantly in lead halide perovskite nanocrystals compared to more common binary systems. For the elemental analysis method, the significant departure of Cs:Pb:X stoichiometric ratio in QDs from the bulk value of 1:1:3 that depends on the size of the QD and on the reaction condition can complicate the determination of the absorption cross section. Because of the labile anion and the sensitivity of the crystal phase to the surrounding environment, lead halide perovskite nanocrystals are more susceptible to change its stoichiometric composition or structure in response to changes of ligand and solvent environment.[40] For instance, Cs/Pb ratio in the range of 0.62 - 1.5 that varies depending on the QD size, synthesis method and aging of the sample was reported.[13, 25, 28, 40, 41] Large deviation of Cs/Pb ratio from 1 that varies with the thickness was also observed in 1D and 2D structures.[2] Br/Pb ratio is also shown to be size dependent, exhibiting increasing Br/Pb ratio with decreasing QD size in the Br-terminated QDs.[41] In the case of $CsPbCl_3$ QDs, post-synthesis self-anion exchange resulted in significant increase of the absorption intensity with concomitant increase of PL quantum yield without noticeable change of the particle size, presumably

by removing the existing Cl vacancies in the QDs.[44] This contrasts to the case of $CsPbBr_3$ QDs, where no change of absorption and PL intensity were observed upon self-anion exchange, which suggests much less halide vacancy in $CsPbBr_3$ QDs than in $CsPbCl_3$ QDs. Because of the large variation of the elemental composition that depends on various factors exemplified above, accuracy of the elemental composition is particularly important in determination of the absorption cross section of lead halide perovskite nanocrystals via elemental analysis. When the uncertainty in volume and elemental composition of the nanocrystals is high, TA saturation method could be more advantageous than the elemental analysis method.

2.4. Conclusions

The absorption cross section is an important spectroscopic parameter of the colloidal QDs crucial to understand their photophysical properties that depend on the density of photoexcited excitons. The absorption cross section of the colloidal QDs has been measured in many different ways including elemental analysis and saturation of transient PL or transient absorption signal, which gave consistent results for various binary semiconductor QDs. However, there is significant discrepancy in the reported absorption cross section values of lead halide perovskite QDs determined by using different methods, notably those determined by the transient PL intensity saturation method being much smaller than those from the elemental analysis. In this work, we made comparative analysis of the absorption cross section of $CsPbBr_3$ QDs of varying sizes, employing elemental analysis and transient absorption (TA) saturation methods to establish more

reliable absorption cross section values. Comparison of the results from this study and previous reports indicates that both the elemental analysis and TA saturation results in consistent absorption cross sections, which are of the same order of magnitude to those of II-VI QDs of the similar volume. We concluded that the absorption cross section determined by elemental analysis and TA saturation are more accurate than those reported previously by using the transient PL saturation method that are smaller by an order of magnitude, although the reason for such large underestimation is not clear.

3. SUMMARY AND OUTLOOK

The linear relationship between $CsPbBr_3$ particle volume and absorption cross section at wavelengths above the optical band edge has been further demonstrated for the quantum confined particles ranging in size from 3.8 nm to just below 7 nm. The transient absorption saturation method employed has shown to have results agreeing with the elemental analysis method also performed and both show agreement with previous studies employing the elemental analysis method. Better understanding the particle volume and absorption cross section relationship has several important implications and benefits for future work. Using the transient absorption saturation method further detailed by the work has helped others quantify different morphologies in the same volume regime investigated for cubic particles.[45] The quantitative cross section analysis has also allowed for ease of prediction of photoexcitation events and concentration analyses for the nanoscale perovskite material.

Overall this work has started to help better understand the physical picture behind many of the perovskite's lauded attributes though much more work remains to be done in order to fundamentally understand the chemistry of the quantum confined semiconductor perovskite to further drive its use cases for a variety of possible optoelectronic, synthetic, catalytic, and energetic applications.

REFERENCES

1. Protesescu, L.; Yakunin, S.; Bodnarchuk, M. I.; Krieg, F.; Caputo, R.; Hendon, C. H.; Yang, R. X.; Walsh, A.; Kovalenko, M. V., Nanocrystals of Cesium Lead Halide Perovskites (CsPbX3, X = Cl, Br, and I): Novel Optoelectronic Materials Showing Bright Emission with Wide Color Gamut. *Nano Lett.* **2015,** *15* (6), 3692-3696.

2. Dong, Y.; Qiao, T.; Kim, D.; Rossi, D.; Ahn, S. J.; Son, D. H., Controlling Anisotropy of Quantum-Confined CsPbBr3 Nanocrystals by Combined Use of Equilibrium and Kinetic Anisotropy. *Chem. Mater.* **2019**.

3. Yettapu, G. R.; Talukdar, D.; Sarkar, S.; Swarnkar, A.; Nag, A.; Ghosh, P.; Mandal, P., Terahertz Conductivity within Colloidal CsPbBr3 Perovskite Nanocrystals: Remarkably High Carrier Mobilities and Large Diffusion Lengths. *Nano Lett.* **2016,** *16* (8), 4838-4848.

4. Dong, Y.; Qiao, T.; Kim, D.; Parobek, D.; Rossi, D.; Son, D. H., Precise Control of Quantum Confinement in Cesium Lead Halide Perovskite Quantum Dots via Thermodynamic Equilibrium. *Nano Lett.* **2018,** *18* (6), 3716-3722.

5. Lan, J.; Luo, L.; Wang, M.; Li, F.; Wu, X.; Wang, F., One pot gram-scale synthesis of CsPbBr3 nanocrystals and their application in green LED. *J. Lumin.* **2019,** *210*, 464-471.

6. Wang, Y.; Li, X. M.; Song, J. Z.; Xiao, L.; Zeng, H. B.; Sun, H. D., All-Inorganic Colloidal Perovskite Quantum Dots: A New Class of Lasing Materials with Favorable Characteristics. *Adv. Mater.* **2015,** *27* (44), 7101-7108.

7. Yakunin, S.; Protesescu, L.; Krieg, F.; Bodnarchuk, M. I.; Nedelcu, G.; Humer, M.; De Luca, G.; Fiebig, M.; Heiss, W.; Kovalenko, M. V., Low-threshold amplified spontaneous emission and lasing from colloidal nanocrystals of caesium lead halide perovskites (vol 6, 8056, 2015). *Nature Communications* **2015,** *6*.

8. Yuan, H. W.; Zhao, Y. Y.; Duan, J. L.; Wang, Y. D.; Yang, X. Y.; Tang, Q. W., All-inorganic CsPbBr3 perovskite solar cell with 10.26% efficiency by spectra engineering. *Journal of Materials Chemistry A* **2018,** *6* (47), 24324-24329.

9. Green, M. A.; Ho-Baillie, A.; Snaith, H. J., The emergence of perovskite solar cells. *Nature Photonics* **2014,** *8*, 506.

10. Burschka, J.; Pellet, N.; Moon, S.-J.; Humphry-Baker, R.; Gao, P.; Nazeeruddin, M. K.; Grätzel, M., Sequential deposition as a route to high-performance perovskite-sensitized solar cells. *Nature* **2013,** *499*, 316.

11. Butkus, J.; Vashishtha, P.; Chen, K.; Gallaher, J. K.; Prasad, S. K. K.; Metin, D. Z.; Laufersky, G.; Gaston, N.; Halpert, J. E.; Hodgkiss, J. M., The Evolution of Quantum Confinement in CsPbBr3 Perovskite Nanocrystals. *Chem. Mater.* **2017,** *29* (8), 3644-3652.

12. Leatherdale, C. A.; Woo, W. K.; Mikulec, F. V.; Bawendi, M. G., On the absorption cross section of CdSe nanocrystal quantum dots. *J. Phys. Chem. B* **2002,** *106* (31), 7619-7622.

13. Maes, J.; Balcaen, L.; Drijvers, E.; Zhao, Q.; De Roo, J.; Vantomme, A.; Vanhaecke, F.; Geiregat, P.; Hens, Z., Light Absorption Coefficient of CsPbBr3 Perovskite Nanocrystals. *J. Phys. Chem. Lett.* **2018,** *9* (11), 3093-3097.

14. Castaneda, J. A.; Nagamine, G.; Yassitepe, E.; Bonato, L. G.; Voznyy, O.; Hoogland, S.; Nogueira, A. F.; Sargent, E. H.; Cruz, C. H. B.; Padilha, L. A., Efficient Biexciton Interaction in Perovskite Quantum Dots Under Weak and Strong Confinement. *ACS Nano* **2016,** *10* (9), 8603-8609.

15. Puthenpurayil, J.; Cheng, O. H. C.; Qiao, T.; Rossi, D.; Son, D. H., On the determination of absorption cross section of colloidal lead halide perovskite quantum dots. *J. Chem. Phys.* **2019,** *151* (15).

16. Giblin, J.; Syed, M.; Banning, M. T.; Kuno, M.; Hartland, G., Experimental Determination of Single CdSe Nanowire Absorption Cross Sections through Photothermal Imaging. *ACS Nano* **2010,** *4* (1), 358-364.

17. Rossi, D.; Liu, X. H.; Lee, Y. J.; Khurana, M.; Puthenpurayil, J.; Kim, K.; Akimov, A. V.; Cheon, J.; Son, D. H., Intense Dark Exciton Emission from Strongly Quantum-Confined CsPbBr3 Nanocrystals. *Nano Lett.* **2020,** *20* (10), 7321-7326.

18. Parobek, D.; Meeder, J. R.; Puthenpurayil, J.; Nippe, M.; Son, D. H., Breaking the short-range proximity requirement in quantum dot/molecular catalyst hybrids for CO2 reduction via long-range hot electron sensitization. *Journal of Materials Chemistry A* **2020,** *8* (26), 12984-12989.

19. Orrison, C.; Meeder, J. R.; Zhang, B. W.; Puthenpurayil, J.; Hall, M. B.; Nippe, M.; Son, D. H., Efficient Redox-Neutral Photocatalytic Formate to Carbon

Monoxide Conversion Enabled by Long-Range Hot Electron Transfer from Mn-Doped Quantum Dots. *Journal of the American Chemical Society* **2021,** *143* (27), 10292-10300.

20. Swarnkar, A.; Marshall, A. R.; Sanehira, E. M.; Chernomordik, B. D.; Moore, D. T.; Christians, J. A.; Chakrabarti, T.; Luther, J. M., Quantum dot–induced phase stabilization of α-CsPbI3 perovskite for high-efficiency photovoltaics. *Science* **2016,** *354* (6308), 92.

21. Beal, R. E.; Slotcavage, D. J.; Leijtens, T.; Bowring, A. R.; Belisle, R. A.; Nguyen, W. H.; Burkhard, G. F.; Hoke, E. T.; McGehee, M. D., Cesium Lead Halide Perovskites with Improved Stability for Tandem Solar Cells. *The Journal of Physical Chemistry Letters* **2016,** *7* (5), 746-751.

22. Tan, Z.-K.; Moghaddam, R. S.; Lai, M. L.; Docampo, P.; Higler, R.; Deschler, F.; Price, M.; Sadhanala, A.; Pazos, L. M.; Credgington, D.; Hanusch, F.; Bein, T.; Snaith, H. J.; Friend, R. H., Bright light-emitting diodes based on organometal halide perovskite. *Nature Nanotechnology* **2014,** *9*, 687.

23. Xing, G.; Mathews, N.; Lim, S. S.; Yantara, N.; Liu, X.; Sabba, D.; Grätzel, M.; Mhaisalkar, S.; Sum, T. C., Low-temperature solution-processed wavelength-tunable perovskites for lasing. *Nature Materials* **2014,** *13*, 476.

24. Yakunin, S.; Protesescu, L.; Krieg, F.; Bodnarchuk, M. I.; Nedelcu, G.; Humer, M.; De Luca, G.; Fiebig, M.; Heiss, W.; Kovalenko, M. V., Low-threshold amplified spontaneous emission and lasing from colloidal nanocrystals of caesium lead halide perovskites. *Nature Communications* **2015,** *6*, 8056.

25. Du, X. F.; Wu, G.; Cheng, J.; Dang, H.; Ma, K. Z.; Zhang, Y. W.; Tan, P. F.; Chen, S., High-quality CsPbBr3 perovskite nanocrystals for quantum dot light-emitting diodes. *Rsc Advances* **2017,** *7* (17), 10391-10396.

26. Dutta, A.; Behera, R. K.; Pal, P.; Baitalik, S.; Pradhan, N., Near-Unity Photoluminescence Quantum Efficiency for All CsPbX3 (X=Cl, Br, and I) Perovskite Nanocrystals: A Generic Synthesis Approach. **2019,** *58* (17), 5552-5556.

27. Han, Y.; Luo, X.; Lai, R.; Li, Y.; Liang, G.; Wu, K., Visible-Light-Driven Sensitization of Naphthalene Triplets Using Quantum-Confined CsPbBr3 Nanocrystals. *The Journal of Physical Chemistry Letters* **2019,** *10* (7), 1457-1463.

28. De Roo, J.; Ibanez, M.; Geiregat, P.; Nedelcu, G.; Walravens, W.; Maes, J.; Martins, J. C.; Van Driessche, I.; Koyalenko, M. V.; Hens, Z., Highly Dynamic Ligand

Binding and Light Absorption Coefficient of Cesium Lead Bromide Perovskite Nanocrystals. *ACS Nano* **2016,** *10* (2), 2071-2081.

29. Wu, K. F.; Liang, G. J.; Shane, Q. Y.; Ren, Y. P.; Kong, D. G.; Lian, T. Q., Ultrafast Interfacial Electron and Hole Transfer from CsPbBr3 Perovskite Quantum Dots. *Journal of the American Chemical Society* **2015,** *137* (40), 12792-12795.

30. Yu, P. R.; Beard, M. C.; Ellingson, R. J.; Ferrere, S.; Curtis, C.; Drexler, J.; Luiszer, F.; Nozik, A. J., Absorption cross-section and related optical properties of colloidal InAs quantum dots. *J. Phys. Chem. B* **2005,** *109* (15), 7084-7087.

31. Yu, W. W.; Qu, L.; Guo, W.; Peng, X., Experimental Determination of the Extinction Coefficient of CdTe, CdSe, and CdS Nanocrystals. *Chem. Mater.* **2003,** *15* (14), 2854-2860.

32. Moreels, I.; Lambert, K.; De Muynck, D.; Vanhaecke, F.; Poelman, D.; Martins, J. C.; Allan, G.; Hens, Z., Composition and size-dependent extinction coefficient of colloidal PbSe quantum dots. *Chem. Mater.* **2007,** *19* (25), 6101-6106.

33. Cademartiri, L.; Montanari, E.; Calestani, G.; Migliori, A.; Guagliardi, A.; Ozin, G. A., Size-Dependent Extinction Coefficients of PbS Quantum Dots. *J. Am. Chem. Soc.* **2006,** *128* (31), 10337-10346.

34. Ji, M. B.; Park, S.; Connor, S. T.; Mokari, T.; Cui, Y.; Gaffney, K. J., Efficient Multiple Exciton Generation Observed in Colloidal PbSe Quantum Dots with Temporally and Spectrally Resolved Intraband Excitation. *Nano Lett.* **2009,** *9* (3), 1217-1222.

35. Makarov, N. S.; Guo, S.; Isaienko, O.; Liu, W.; Robel, I.; Klimov, V. I., Spectral and Dynamical Properties of Single Excitons, Biexcitons, and Trions in Cesium–Lead-Halide Perovskite Quantum Dots. *Nano Lett.* **2016,** *16* (4), 2349-2362.

36. de Mello Donegá, C.; Koole, R., Size Dependence of the Spontaneous Emission Rate and Absorption Cross Section of CdSe and CdTe Quantum Dots. *J. Phys. Chem. C* **2009,** *113* (16), 6511-6520.

37. Rossi, D.; Wang, H.; Dong, Y.; Qiao, T.; Qian, X.; Son, D. H., Light-Induced Activation of Forbidden Exciton Transition in Strongly Confined Perovskite Quantum Dots. *ACS Nano* **2018,** *12* (12), 12436-12443.

38. de Araújo, M. A.; Silva, R.; de Lima, E.; Pereira, D. P.; de Oliveira, P. C., Measurement of Gaussian laser beam radius using the knife-edge technique: improvement on data analysis. *Appl. Opt.* **2009,** *48* (2), 393-396.

39. Weidman, M. C.; Seitz, M.; Stranks, S. D.; Tisdale, W. A., Highly Tunable Colloidal Perovskite Nanoplatelets through Variable Cation, Metal, and Halide Composition. *ACS Nano* **2016,** *10* (8), 7830-7839.

40. Bodnarchuk, M. I.; Boehme, S. C.; ten Brinck, S.; Bernasconi, C.; Shynkarenko, Y.; Krieg, F.; Widmer, R.; Aeschlimann, B.; Gunther, D.; Kovalenko, M. V.; Infante, I., Rationalizing and Controlling the Surface Structure and Electronic Passivation of Cesium Lead Halide Nanocrystals. *ACS Energy Lett.* **2019,** *4* (1), 63-74.

41. Dong, Y. T.; Qiao, T.; Kim, D.; Parobek, D.; Rossi, D.; Son, D. H., Precise Control of Quantum Confinement in Cesium Lead Halide Perovskite Quantum Dots via Thermodynamic Equilibrium. *Nano Lett.* **2018,** *18* (6), 3716-3722.

42. Park, Y.-S.; Guo, S.; Makarov, N. S.; Klimov, V. I., Room Temperature Single-Photon Emission from Individual Perovskite Quantum Dots. *ACS Nano* **2015,** *9* (10), 10386-10393.

43. Chen, H.-Y.; Chen, T.-Y.; Berdugo, E.; Park, Y.; Lovering, K.; Son, D. H., Hot Electrons from Consecutive Exciton–Mn Energy Transfer in Mn-Doped Semiconductor Nanocrystals. *The Journal of Physical Chemistry C* **2011,** *115* (23), 11407-11412.

44. Parobek, D.; Dong, Y.; Qiao, T.; Rossi, D.; Son, D. H., Photoinduced Anion Exchange in Cesium Lead Halide Perovskite Nanocrystals. *Journal of the American Chemical Society* **2017,** *139* (12), 4358-4361.

45. Zhang, F. Y.; Liu, Y. C.; Wei, S. Q.; Chen, J. S.; Zhou, Y.; He, R. X.; Pullerits, T.; Zheng, K. B., Microscopic morphology independence in linear absorption cross-section of CsPbBr3 nanocrystals. *Science China-Materials* **2021,** *64* (6), 1418-1426.

46. Jang, D. M.; Kim, D. H.; Park, K.; Park, J.; Lee, J. W.; Song, J. K., Ultrasound synthesis of lead halide perovskite nanocrystals. *Journal of Materials Chemistry C* **2016,** *4* (45), 10625-10629.

47. Akkerman, Q. A.; D'Innocenzo, V.; Accornero, S.; Scarpellini, A.; Petrozza, A.; Prato, M.; Manna, L., Tuning the Optical Properties of Cesium Lead Halide

Perovskite Nanocrystals by Anion Exchange Reactions. *Journal of the American Chemical Society* **2015,** *137* (32), 10276-10281.

48. Tong, Y.; Bladt, E.; Ayguler, M. F.; Manzi, A.; Milowska, K. Z.; Hintermayr, V. A.; Docampo, P.; Bals, S.; Urban, A. S.; Polavarapu, L.; Feldmann, J., Highly Luminescent Cesium Lead Halide Perovskite Nanocrystals with Tunable Composition and Thickness by Ultrasonication. *Angewandte Chemie-International Edition* **2016,** *55* (44), 13887-13892.

APPENDIX A

SUPPLEMENTARY MATERIAL OF CHAPTER 2

1. Pump fluence determination

Pump beam was approximated as Gaussian beams with the following intensity profile.

$$I(r) = I_0 \exp\left(\frac{-2r^2}{\omega_0^2}\right) \quad (5)$$

Where $I(r)$ is the intensity at a given distance r from the center of the beam. I_0 is the peak intensity. ω_0 is the Gaussian beam radius, at which the intensity decreases to $1/e^2$ of its peak value. The average fluence of pump pulse under the probe area defined as the circular region with diameter of fwhm of the probe beam ($fwhm = 2R_{pr}$) was calculated as follows.

$$Average\ Fluence = \frac{2\pi \int_0^{R_{pr}} I_0 \exp\left(\frac{-2r^2}{\omega_0^2}\right) r dr}{\pi {R_{pr}}^2 (pulse\ repetition\ rate)}$$

$$= \frac{P_{tot}\left[1 - \exp\left(\frac{-2{R_{pr}}^2}{\omega_0^2}\right)\right]}{(\pi {R_{pr}}^2)(pulse\ repetition\ rate)} \quad (2)$$

P_{tot} is the total power of the pump beam.

2. Elemental analysis and determination of molar concentration of QDs

The number of unit cells (unit cell edge length = 0.5874 nm[S1, 46-48]) in the cube-shaped $CsPbBr_3$ QDs of volume V_{QD} was calculated first using the size of the QD determined from TEM.

$$N_{unit\ cell} = \frac{V_{QD}}{V_{unit\ cell}} \quad (3)$$

Using one Pb atom per unit cell, the total number of QDs in the sample (N_{QD}) is obtained from

$$N_{QD} = \frac{N_{Pb}}{N_{unit\ cell}} \quad (4)$$

The total number of Pb in the sample (N_{Pb}) was determined from the elemental analysis.

The molar concentration of the QDs (c) was determined from the following expression, where V_{sample} is the volume of the QD sample solution used to obtain the absorption spectrum. N_A is the Avogadro's number.

$$c = \frac{N_{QD}}{N_A\, V_{sample}} \quad (5)$$

QD edge length, L (nm)	$N_{unit\ cell}$
3.8	271
5.0	617
5.9	1013
6.9	1621

Table S1. The number of unit cells per $CsPbBr_3$ QDs with different edge length (L). The volume of QD is $V_{QD} = L^3$.

3. Comparison of the absorption cross sections (in cm^2) of $CsPbBr_3$ QDs from this work and literature

QD size (nm)	TA saturation (This work)	Elemental analysis (This work)	Elemental analysis (Ref S[13])	PL saturation (Ref S[14])	PL saturation (Ref S[35])	PL saturation (Ref S[6])
3.8	4.5×10^{-15}	4.4×10^{-15}	-	-	-	-
4.1	-	4.7×10^{-15}	5.3×10^{-15}	-	-	-
4.2	-	6.5×10^{-15}	-	-	-	-
4.5	7.5×10^{-15}	-	-	-	-	-
5.0	1.0×10^{-14}	1.0×10^{-14}	-	-	-	-
5.4	1.1×10^{-14}	-	-	-	-	-
5.8	1.7×10^{-14}	-	1.5×10^{-14}	-	-	-
5.9	-	2.0×10^{-14}	-	1.0×10^{-15}	-	-
6.3	-	-	-	-	3.5×10^{-15}	-
6.4	2.0×10^{-14}	-	-	-	-	-
6.9	3.2×10^{-14}	3.4×10^{-14}	-	-	-	-
7.0	-	-	-	1.4×10^{-15}	-	-
7.1	-	-	-	2.0×10^{-15}	-	-
7.3	-	-	3.0×10^{-14}	-	-	-
8.1	-	-	-	-	8.0×10^{-15}	-
8.3	-	-	4.4×10^{-14}	-	-	-
9.0	-	-	-	-	-	2.5×10^{-14}
9.3	-	-	-	-	1.3×10^{-14}	-
10.8	-	-	9.7×10^{-14}	-	-	-
13.1	-	-	-	1.4×10^{-14}	-	

Table S2. Selected 400 nm absorption cross section values in cm^2.

4. Plot of the absorption cross section of $CsPbBr_3$ QDs of different sizes from this work.

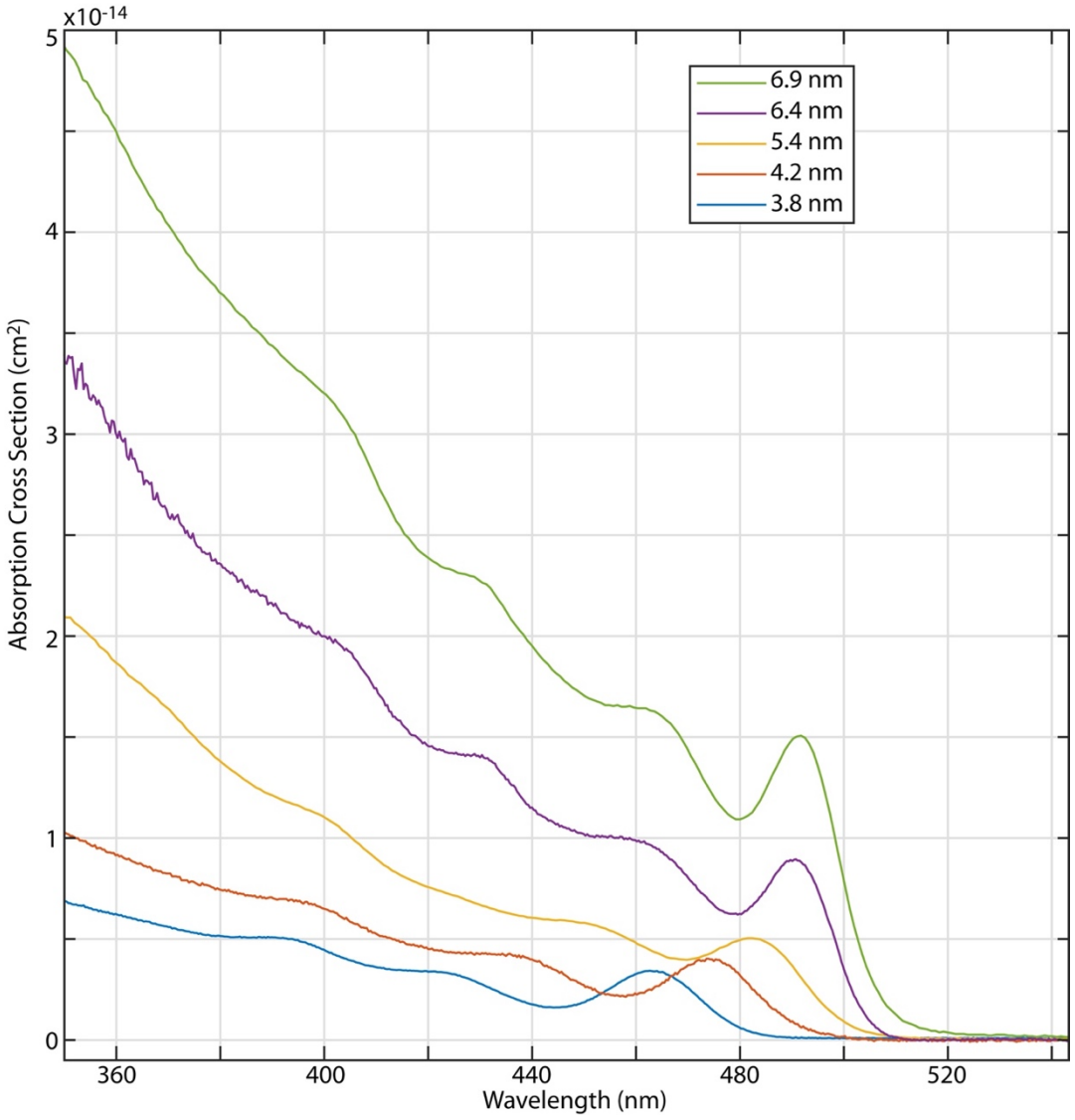

Figure S1. Absorption cross sections of $CsPbBr_3$ QDs with different edge lengths.

QD Size (nm)	400 nm Absorption Cross Section (cm^2)	Band Edge Wavelength (nm)	Band Edge Absorption Cross Section (cm^2)
3.8	$4.5x10^{-15}$	463	$3.4x10^{-15}$
4.2	$6.5x10^{-15}$	474	$4.0x10^{-15}$
5.4	$1.1x10^{-14}$	482	$5.0x10^{-15}$
6.4	$2.0x10^{-14}$	490	$8.9x10^{-15}$
6.9	$3.2x10^{-14}$	492	$1.5x10^{-14}$

Table S3. Comparison of band edge absorption cross sections in cm^2 for selected QD sizes.

5. Pump fluence-dependent transient absorption (TA) data of $CsPbBr_3$ QDs of different sizes and fit of the TA saturation to the Eq. (4) in the manuscript.

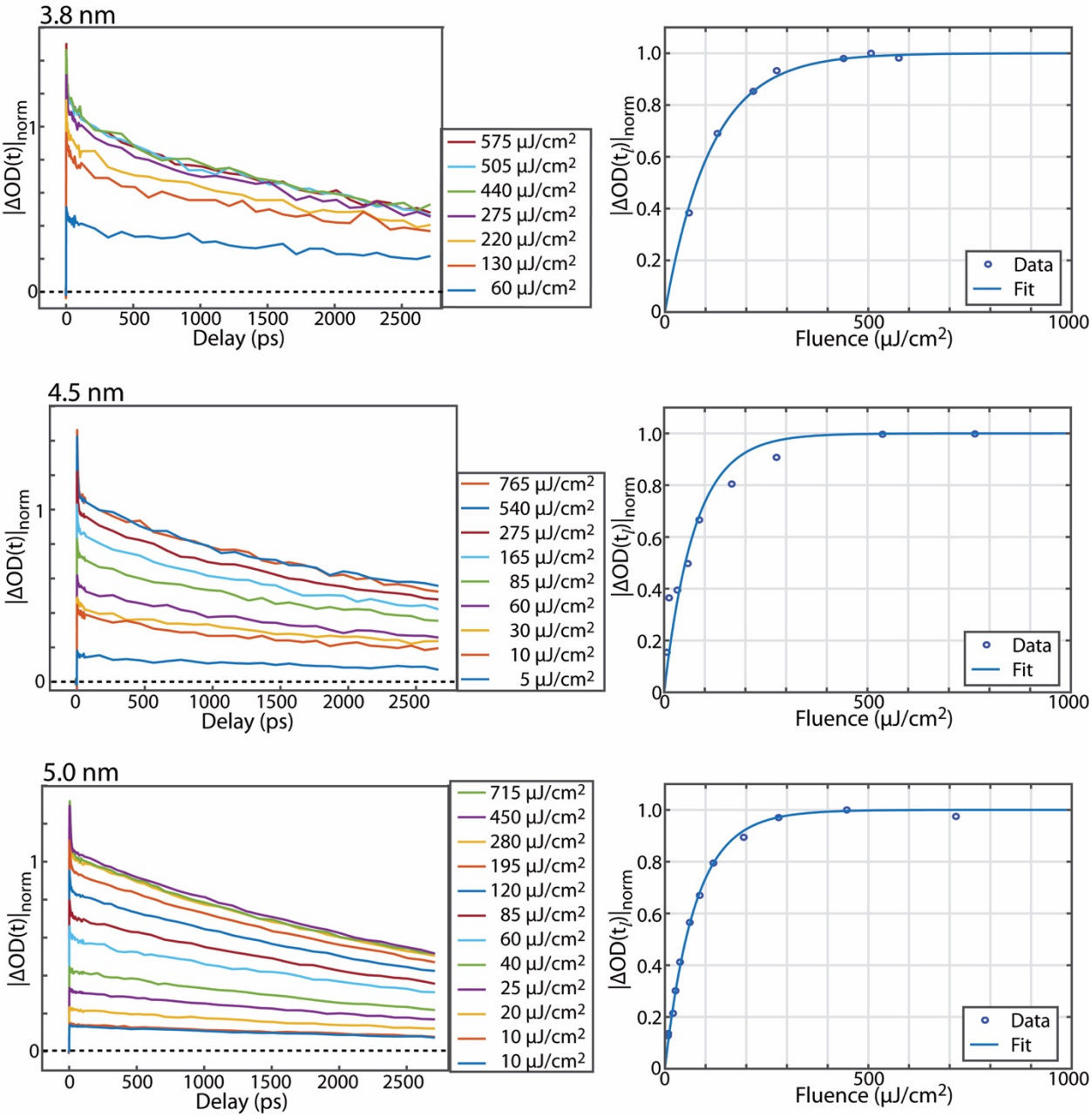

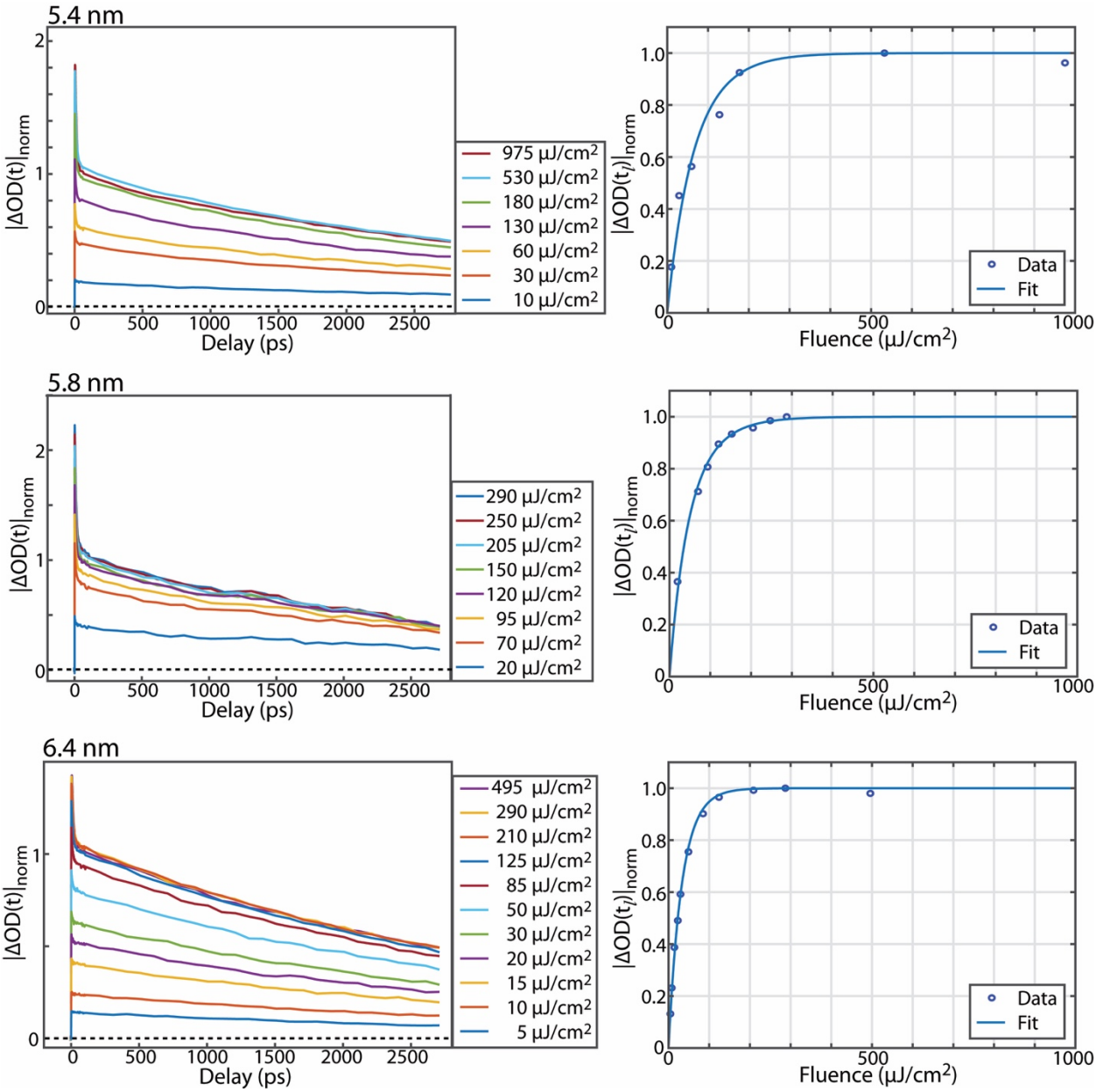
5.4 nm
|ΔOD(t)|norm
Delay (ps)
975 μJ/cm2
530 μJ/cm2
180 μJ/cm2
130 μJ/cm2
60 μJ/cm2
30 μJ/cm2
10 μJ/cm2
|ΔOD(tf)|norm
Fluence (μJ/cm2)
Data
Fit
5.8 nm
290 μJ/cm2
250 μJ/cm2
205 μJ/cm2
150 μJ/cm2
120 μJ/cm2
95 μJ/cm2
70 μJ/cm2
20 μJ/cm2
6.4 nm
495 μJ/cm2
290 μJ/cm2
210 μJ/cm2
125 μJ/cm2
85 μJ/cm2
50 μJ/cm2
30 μJ/cm2
20 μJ/cm2
15 μJ/cm2
10 μJ/cm2
5 μJ/cm2

6. Derivation of Eq. (4) in the manuscript.

x-dependent pump photon fluence at location *x* along the beam path within the sample in the cell of pathlength *l* is as follows. F_0 is the incident photon fluence at the front of the sample cell, A_l is the absorbance of the sample in the cell.

$$F_{ph}(A_l, x, l, F_0) = F_0 \cdot 10^{-A_l(x/l)} \tag{6}$$

$|\Delta OD(t_l)|_{norm}$ averaged over the range of $0 \leq x \leq l$ is as follows, where $x' = x/l$. σ_λ is the absorption cross section at wavelength λ.

$$|\Delta OD(t_l)|_{norm} = \int_0^1 (1 - e^{-F_0 * \left(10^{-A_l(x')}\right) * \sigma_\lambda}) dx' \tag{7}$$

$$= \frac{-E_1(\sigma_\lambda \cdot F_0 \cdot 10^{-A_l}) + E_1(\sigma_\lambda \cdot F_0)}{A_l \cdot ln(10)} + 1, \quad E_1(x) = \int_x^\infty \frac{e^{-u}}{u} du$$

Additional Supporting Information:

Overlap Intensity Derivation

Gaussian Beams have the following intensity (units of W/m^2) distribution:

$$I(r) = I_0 \exp\left(\frac{-2r^2}{\omega_0^2}\right)$$

I_0 = Peak Intensity

I(r) = Intensity at a given distance (radius) from center

r = radius, distance from center

ω_0 = Gaussian beam radius, radius at which intensity has decreased to $1/e^2$ (0.135) of its initial value

The Gaussian beam radius can be related to the radius at half maximum

Radius at half maximum = $0.59\omega_0$

FWHM = $2(0.59)\omega_0$

The power contained within a radius, r, can then be found by integrating the intensity distribution:

$$P(r) = P(\infty)[1 - \exp\left(\frac{-2r^2}{\omega_0^2}\right)]$$

P(r) = Power contained within a radius, r

P(∞) = Total power of the beam (units of W)

The area of a circle is:

$$Area = \pi r^2$$

Knowing the power contained within a radius and the radius, expressions can be combined to give intensity within a radius in W/m^2:

$$Intensity_{radius} = \frac{(P(\infty)[1 - \exp\left(\frac{-2r^2}{\omega_0^2}\right)])}{\pi r^2}$$

Then the intensity within a radius can be converted to fluence (J/m^2), knowing the repetition rate ($Hz = s^{-1}$) of the laser

$$Fluence = \frac{Intensity_{radius}}{RepititionRate}$$

Plotting TA signal against the fluence gives a curve that can be fit to:

$$1 - \exp(-Fluence * C)$$

C = Absorption Cross Section

The absorption cross section can then be extracted from this curve.

Intensity Distribution Integration

The Peak intensity, I_0, is related to the total power, $P(\infty)$:

$$I_0 = \frac{2P(\infty)}{\pi\omega_0^2}$$

The intensity distribution is:

$$I(r) = I_0 \exp\left(\frac{-2r^2}{\omega_0^2}\right)$$

Integrating over a circular area uses:

$$dArea = rdrd\theta$$

Setting up the integral gives:

$$\int_0^r \int_0^{2\pi} I_0 \exp\left(\frac{-2r^2}{\omega_0^2}\right) r\,dr\,d\theta$$

Splitting up and integrating gives:

$$I_0\left[\frac{-\omega_0^2}{4}\exp\left(\frac{-2r^2}{\omega_0^2}\right)\right]_0^r \int_0^{2\pi} d\theta$$

Solving gives:

$$I_0 \frac{-\omega_0^2}{4}\left(\exp\left(\frac{-2r^2}{\omega_0^2}\right) - 1\right)2\pi$$

Plugging in for I_0:

$$\left(\frac{2P(\infty)}{\pi\omega_0^2}\right)\frac{-\omega_0^2}{4}\left(\exp\left(\frac{-2r^2}{\omega_0^2}\right) - 1\right)2\pi$$

Canceling:

$$-P(\infty)\left(\exp\left(\frac{-2r^2}{\omega_0^2}\right)-1\right)$$

Distributing and Rearranging:

$$P(\infty)\left[1-\exp\left(\frac{-2r^2}{\omega_0^2}\right)\right]$$